Fuel 234 (2018) 189–198

Contents lists available at ScienceDirect

Fuel

journal homepage: www.elsevier.com/locate/fuel

Full Length Article

Numerical study of particle deposition in turbulent duct flow with a forward- or backward-facing step

Hao Lu[a,b], Wenjun Zhao[c,*]

[a] Key Laboratory of Enhanced Heat Transfer and Energy Conservation of Education Ministry, School of Chemistry and Chemical Engineering, South China University of Technology, Guangzhou 510640, China
[b] Faculty of Engineering, The University of Nottingham, Nottingham, United Kingdom
[c] Faculty of Architecture, The University of Hong Kong, Hong Kong, China

ARTICLE INFO

Keywords:
Particle deposition
Forward-facing step
Backward-facing step
Numerical simulation

ABSTRACT

Particle deposition in duct air flow over a forward- or backward-facing step was investigated by Reynolds stress model with velocity fluctuation correction combined with discrete particle model. The mean air velocities in duct with a backward-facing step and particle deposition velocities for smooth duct both agreed well with related literature results. The deposition velocities of the duct with a forward-facing step are significantly higher than those of smooth duct, especially for small particles ($d_p < 10\,\mu$m). Particle deposition velocities in the duct with a backward-facing step are higher for small particles ($d_p < 10\,\mu$m) but lower for large particles ($d_p > 10\,\mu$m), compared with smooth duct case. Air velocity and turbulent kinetic energy fields in the duct with a forward- or backward-facing step are quite different from smooth duct case, which modify the particle deposition characteristics significantly. Furthermore, a particle deposition efficiency ratio was defined and analyzed by considering flow drag of the duct. The results showed that the peak deposition efficiency ratio of the duct with a forward-facing step can reach 60 for particles of 1 μm. The duct with a forward-facing step can enhance deposition of small particles more significantly ($d_p < 10\,\mu$m), compared with the duct with a backward-facing step.

1. Introduction

Particulate matter (PM) deposition in turbulent duct flow is usually encountered in energy and environmental engineering. Forward-facing step (FFS) and backward-facing step (BFS) are commonly used in the above gas-particle two-phase devices, such as expansion or contraction of building ventilation duct, the external casing of air cleaner, pulverized coal combustor and gas-particle reactor [1–3]. Moreover, FFS and BFS are basic and important configurations to investigate particle motion behaviors in geometry-induced flow separation. Better understanding of particle deposition characteristics and mechanisms in FFS or BFS flows is significant for efficiency improvement of above related equipment [4–7]. Although a large amount of studies were conducted on particle deposition in smooth duct flow, very limited attention has been paid for deposition behaviors of particles in FFS or BFS flow. Therefore, particle deposition in FFS and BFS duct needs to be investigated in details for better design of many related devices.

In the last several decades, particle deposition in smooth duct flow has been studied by theoretical analysis, experimental measurement and numerical simulation [8–12]. It has been concluded that deposition velocity profile of particles would firstly fall, then significantly rise and finally keep constant as particle relaxation time increases [13–15]. Generally, particle deposition in vertical smooth duct could be separated into three regimes [16]. Particle deposition is determined by turbulent vortex and Brownian diffusion in turbulent particle diffusion regime. With increase of particle diameter, Brownian diffusion effect reduces while particle inertia becomes more important for particle deposition in eddy diffusion-impaction regime. Particle deposition behaviors are mainly dominated by particle inertia due to high mass in inertia-moderated regime. Moreover, Lai et al. [17] developed an empirical model to estimate particle deposition velocity in smooth duct flow. Turbulent particle diffusion, Brownian diffusion and gravity effect were considered in the model. Zhao and Wu [18–19] improved the three-layer model by considering turbuphoresis to model particle deposition behaviors in smooth and rough duct flows.

Recently, CFD simulation becomes a main way to predict particle deposition behaviors in duct flow [20–22]. The Reynolds-averaged Navier-Stokes (RANS) model and discrete particle model (DPM) are

* Corresponding author.
E-mail address: zhaowenjunhku@gmail.com (W. Zhao).

https://doi.org/10.1016/j.fuel.2018.07.033
Received 11 March 2018; Received in revised form 14 June 2018; Accepted 7 July 2018

usually employed to simulate particle deposition in turbulent duct flow [20–22]. Because this Eulerian-Lagrangian method can effectively reflect particle motion behaviors in turbulent flow fields. Tian [23] compared particle deposition velocity in smooth duct by using various RANS models. The results showed Reynolds stress model (RSM) has better accuracy on particle deposition simulation than other RANS models. Zhang et al. [24] found that near-wall treatment is crucial for accurately model particle deposition in smooth duct flow.

Although particle deposition in smooth duct was well investigated, the researches for non-smooth duct case are very limited. Sippola et al. [25–36] experimentally investigated particle deposition rates in S-shape connector and bent duct. Particle deposition velocity in non-smooth duct is obviously higher compared with smooth duct. Lustfeld et al. [27] studied multilayer deposition of particles in FFS duct by experimental measurement. They found that gravitational settling and inertial impaction are the main mechanisms for particle deposition. Benedetto et al. [28] investigated dust dispersion in turbulent flow fields within a 20 L bomb. The results showed that turbulent vortices produce dead volumes for the dust and the dust is pushed toward the walls of the sphere. Moreover, Sarli et al. [29,30] further investigated effects of different nominal particle concentrations and particle diameter on dust dispersion inside a 20 L bomb. They found that sedimentation prevails when the dust nominal concentration is increased and dust is mainly concentrated at the vessel walls with increase of dust diameter. The authors [31–34] previously investigated particle deposition in expanding, contracting and ribbed ducts. We found that particle deposition characteristics in non-smooth duct are greatly different from smooth duct. In consequence, particle deposition in FFS or BFS ducts has been seldom studied and the detailed deposition mechanisms remain unclear. Thus the objective of the study is to examine particle deposition behaviors and mechanisms in FFS and BFS duct flows. The RSM model with user-defined function (UDF) and DPM model were used to simulate turbulent flow and particle movement respectively. Turbulent flow fields, particle deposition velocities and mechanisms in FFS and BFS ducts were studied in details. Moreover, particle deposition efficiency considering flow drag for FFS and BFS ducts was also obtained and compared with smooth duct case, as FFS or BFS may be a potential way to enhance particle deposition in related devices.

2. Numerical methods and solution strategies

The commercial CFD software ANSYS FLUENT 15.0 was used to solve the Reynolds stress model (RSM) turbulence model and discrete particle model (DPM) in the simulation. Moreover, correction of turbulent velocity fluctuation as well as fully developed turbulent inlet velocity and turbulent kinetic energy profiles were imposed in the simulation to improve prediction accuracy by user-defined function codes.

2.1. Reynolds stress model with UDF correction

The Reynolds-averaged Navier-Stokes equation for turbulent duct flow can be written as follows,

$$\frac{\partial \overline{u}_i}{\partial x_i} = 0, \tag{1}$$

$$\frac{\partial \overline{u}_i}{\partial t} + \overline{u}_j \frac{\partial \overline{u}_i}{\partial x_j} = -\frac{1}{\rho}\frac{\partial \overline{p}}{\partial x_i} + \frac{1}{\rho}\frac{\partial}{\partial x_j}\left(\mu \frac{\partial \overline{u}_i}{\partial x_j} - \rho \overline{u_i' u_j'}\right), \tag{2}$$

In the above equations, $\bar{u}_i$ and $\bar{p}$ are velocity and pressure respectively. $\rho \overline{u_i' u_j'}$ is Reynolds stress tensor. Reynolds stress model (RSM) was used in the simulation, as it has been proven to have the best accuracy for predicting particle deposition in RANS models. The transport equation of Reynolds stress can be written by,

$$\frac{\partial}{\partial t}(\overline{u_i' u_j'}) + \bar{u}_k \frac{\partial}{\partial x_k}(\overline{u_i' u_j'}) = \frac{\partial}{\partial x_k}\left(\frac{\nu_t}{\sigma_k}\frac{\partial \overline{u_i' u_j'}}{\partial x_k}\right) - \left(\overline{u_i' u_k'}\frac{\partial \bar{u}_j}{\partial x_k} + \overline{u_j' u_k'}\frac{\partial \bar{u}_i}{\partial x_k}\right) - C_1 \frac{\varepsilon}{k}\left[\overline{u_i' u_j'} - \frac{2}{3}\delta_{ij} k\right] - C_2 [P_{ij} - \frac{2}{3}\delta_{ij} P] - \frac{2}{3}\delta_{ij}\varepsilon \tag{3}$$

Particle turbulent dispersion caused by turbulent instantaneous fluctuation is an important mechanism to affect particle deposition velocity. Discrete Random Walk Model (DRW) was commonly used to simulate particle turbulent dispersion. The DRW model allows successive encounter of particles with turbulent eddies by a Gaussian distributed random velocity fluctuation of fluids and a time scale of turbulent eddy [23]. The turbulent fluctuating velocity is given as,

$$u' = \zeta u'_{rms},\ v' = \zeta v'_{rms},\ w' = \zeta w'_{rms} \tag{4}$$

where ζ is normal distributed random number with zero mean and unit variance; and u'_{rms}, v'_{rms} and w'_{rms} are fluctuating velocities obtained by the RSM model respectively. However, as a time-averaged turbulence model, the RSM model cannot accurately predict particle turbulent dispersion. Thus the correction of turbulent velocity fluctuation is necessary to improve simulation accuracy. Tian et al. [23] numerical predicted particle deposition velocity in smooth duct flow. They found that wall-normal turbulent velocity fluctuation in the near-wall region is crucial for accurately predicting particle deposition velocity. Therefore, the DNS results of wall-normal velocity fluctuation by Kim et al. [35] was employed in particle deposition simulation for smooth duct, as follows,

$$\frac{v'_{rms}}{u^*} = C(y^+)^2,\ \text{for } y^+ < 4 \tag{5}$$

For complex wall turbulent flow, Eq. (6) was successfully used by Lecrivain et al. [36] to improve particle deposition simulation in duct flow with ribs. This equation was also adopted in the present study for FFS and BFS duct cases. The Eq. (6) can be written by,

$$\frac{v'_{rms}}{u^*} = \frac{a_1 y^{+2}}{1 + b_1 y^+ + c_1 y^{+2.41}},\ \text{for } y^+ < 30 \tag{6}$$

In the above equations, $C = 0.008$, $a_1 = 0.0116$, $b_1 = 0.203$ and $c_1 = 0.0014$ y^+ is described by,

$$y^+ = \frac{y\, u^*}{\nu} \tag{7}$$

Turbulent velocity field and TKE distribution have great influences on particle deposition behaviors. Particle deposition characteristics will be quite different in developing and fully developed turbulent duct flow. As particle deposition in fully developed turbulent flows have a lot of engineering applications such as building ventilation system and pneumatic conveying, this study focused on particle deposition in fully developed turbulent flow over a BFS or FFS. Moreover, most of previous studies on particle deposition in turbulent duct flow were in the condition of fully developed turbulent flow status. Thus a large number of experimental and numerical data can be used to validate present numerical methods and results.

Fully developed velocity distributions were obtained and applied at inlet, which can be addressed by [23],

$$U = U_{free}\left(\frac{y}{D/2}\right)^{1/7} \text{for } y \leqslant D/2 \tag{8}$$

$$U = U_{free}\left(\frac{h-y}{D/2}\right)^{1/7} \text{for } y > D/2 \tag{9}$$

$$U_{free} = \frac{8}{7} U_{mean} \tag{10}$$

where D is duct inlet height. U_{mean} is air mean velocity. Pressure outlet and non-slip conditions were employed at outlet and the duct walls. Moreover, fully developed TKE distributions were used at inlet and can

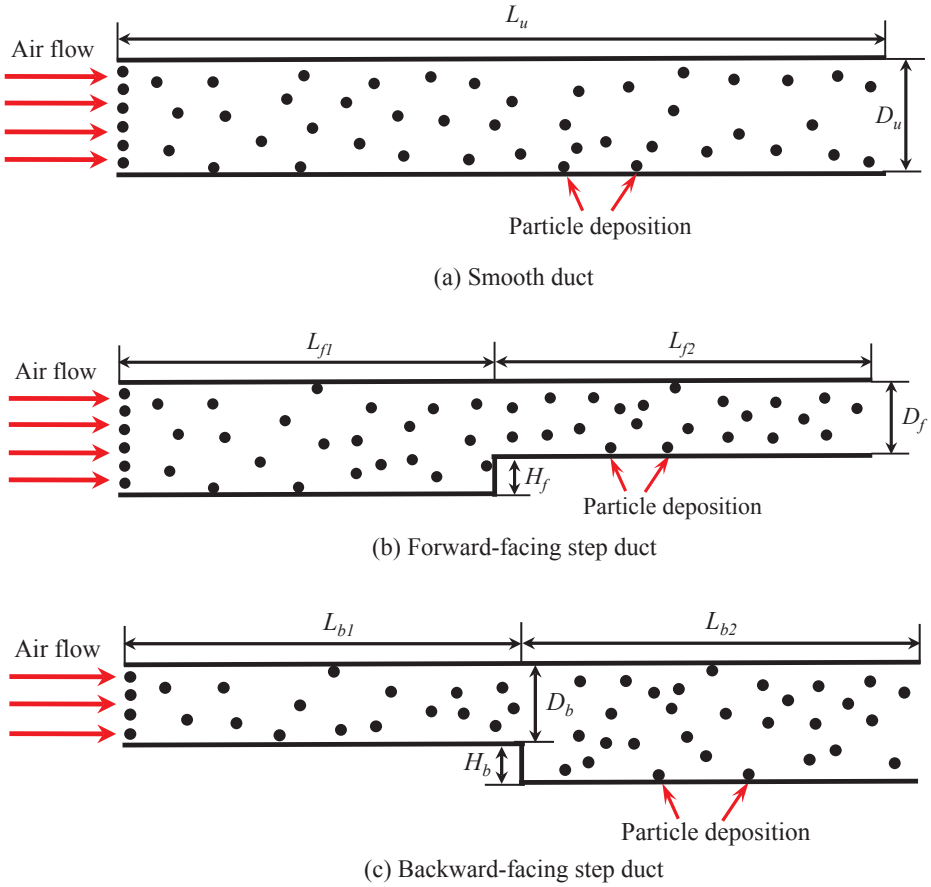

Fig. 1. Schematic of particle deposition in smooth, FFS and BFS ducts.

be demonstrated by [23],

$$k = \frac{\tau_w}{\rho_g\sqrt{C_\mu}} + \frac{y}{D/2}\left(0.002U_{free}^2 - \frac{\tau_w}{\rho_g\sqrt{C_\mu}}\right) \text{ for } 0 \leqslant y \leqslant D/2 \tag{11}$$

$$k = \frac{\tau_w}{\rho_g\sqrt{C_\mu}} + \frac{D-y}{D/2}\left(0.002U_{free}^2 - \frac{\tau_w}{\rho_g\sqrt{C_\mu}}\right) \text{for } D/2 < y \leqslant D \tag{12}$$

$$\tau_w = \frac{\rho_g U_{mean}^2}{2}\cdot f \tag{13}$$

2.2. Discrete particle model considering turbulent dispersion

Discrete particle model (DPM) was used to predict particle movements in air flow fields. As the two-phase flow is quite dilute in this study, influences of particle motion on flow fields and the collision between particles are ignored. In DPM model, particle motion and diffusion are predicted by considering different particle forces. The drag force, the gravity and buoyancy forces, the Brownian force and the Saffman's lift force were modeled in the simulation, which was widely used by a large number of studies on particle deposition prediction, such as Tian and Ahmadi [23], Zhang and Chen [24]. The particle motion equation can be written by [23],

$$\frac{du_p}{dt} = \frac{1}{\tau}\frac{C_D\mathrm{Re}_p}{24}(u_g - u_p) + \frac{g(\rho_p - \rho_g)}{\rho_p} + \zeta\sqrt{\frac{\pi S_0}{\Delta t}} + \frac{2\rho K_c\nu^{0.5}}{\rho_p d_p(S_{lk}S_{kl})}s_{ij}(u - u_p) \tag{14}$$

The drag coefficient C_D was computed as follows,

$$C_D = \frac{24}{\mathrm{Re}_p}, \text{ for } \mathrm{Re}_p < 1 \tag{15}$$

and

$$C_D = \frac{24}{\mathrm{Re}_p}(1 + 0.15\mathrm{Re}_p^{0.687}), \text{ for } 1 < \mathrm{Re}_p < 400 \tag{16}$$

The Stokes number is a crucial parameter in gas-particle flow, which can be defined as [23],

$$St = \frac{\tau_p}{\tau_f} \tag{17}$$

where τ_p is particle relaxation time and τ_f is the characteristic time of the fluid flow. Particle relaxation time τ was computed by [23],

$$\tau_p = \frac{Sd_p^2C_C}{18\nu} \tag{18}$$

where C_C is Cunningham slip correction factor. S is the ratio of particle density to fluid density. Moreover, discrete random walk (DRW) model was used to simulate turbulent dispersion of particles, as it is significant for correctly modelling particle deposition rates [24]. Once the distance of particle barycenter and duct walls is less than particle radius, particles will be deposited on the surfaces. The rebound of particles was not considered in the study, which was in consistent with the studies of Tian [23] and Zhang [24]. As the two-phase flow in present study is quite dilute, particles are sparsely deposited on the duct walls and the deposition region cannot reach packing limit. Therefore, multi-layer deposition was not considered in the study.

2.3. Solution strategies

The steady Reynolds-averaged Navier-Stokes equations were solved

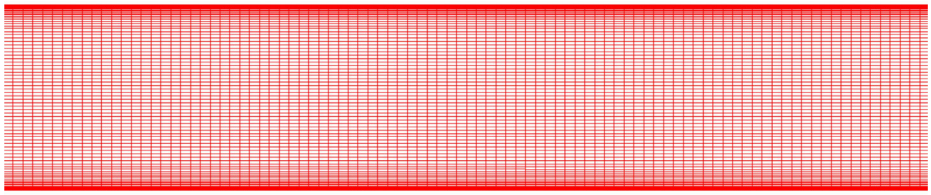

(a) Smooth duct

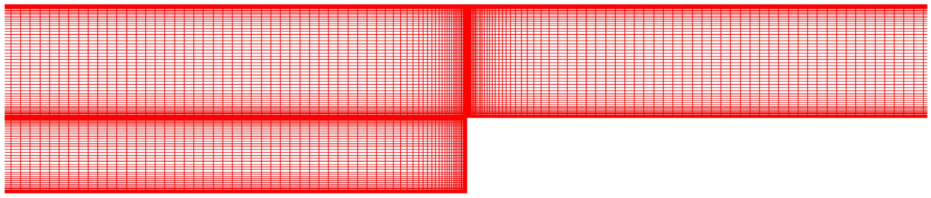

(b) Forward facing step duct

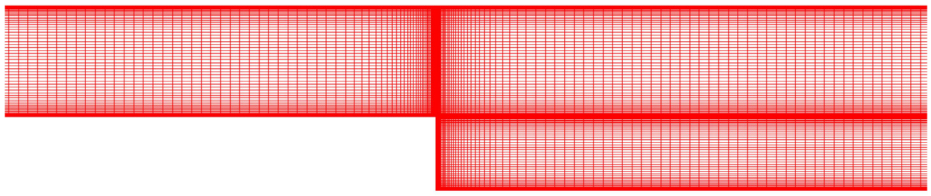

(c) Backward facing step duct

Fig. 2. Partial structural meshes for smooth, FFS and BFS ducts.

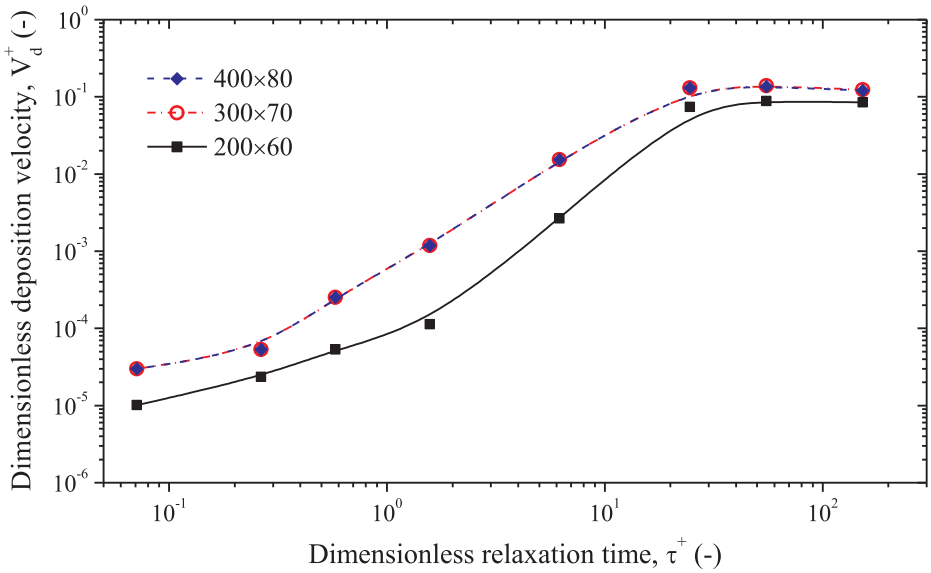

Fig. 3. Comparison of particle deposition velocities in smooth duct with different grid resolution.

by using finite volume method. The pressure and velocity fields were resolved by the Semi-Implicit Method for Pressure Linked Equations (SIMPLE) method [37]. Particle governing equation was resolved by the Runge-Kutta arithmetic.

3. Case description and computational grids

The schematic of particle deposition in smooth, FFS and BFS ducts was shown in Fig. 1(a–c). For smooth duct, the length is 0.4 m and the width is 0.02 m as shown in Fig. 1(a), which is consistent with Tian [23] and Zhang [24] for numerical validation. For FFS and BFS ducts, the first half ducts are uniform while the FFS or BFS was arranged in the middle position of the duct, as shown in Fig. 1(b) and (c). The inlet width and the length of the FFS and BFS ducts are the same with smooth duct. The expanding ratio of the BFS duct was 5:3 while the contracting ratio of the FFS duct was 3:5. The air velocity is 5.5 m/s. The air density is 1.225 kg/m^3 and the air dynamic viscosity μ is 1.789 $\times$ 10^{-5} kg s/m. 30,000 spherical particles were freed from the inlet for smooth, FFS and BFS ducts. The released particle velocities were equal to the mean air velocity. The particle density is 2250 kg/m^3 and particle diameters are 1, 2, 3, 5, 10, 20, 30 and 50 μm.

Partial structured meshes were developed for smooth, FFS and BFS

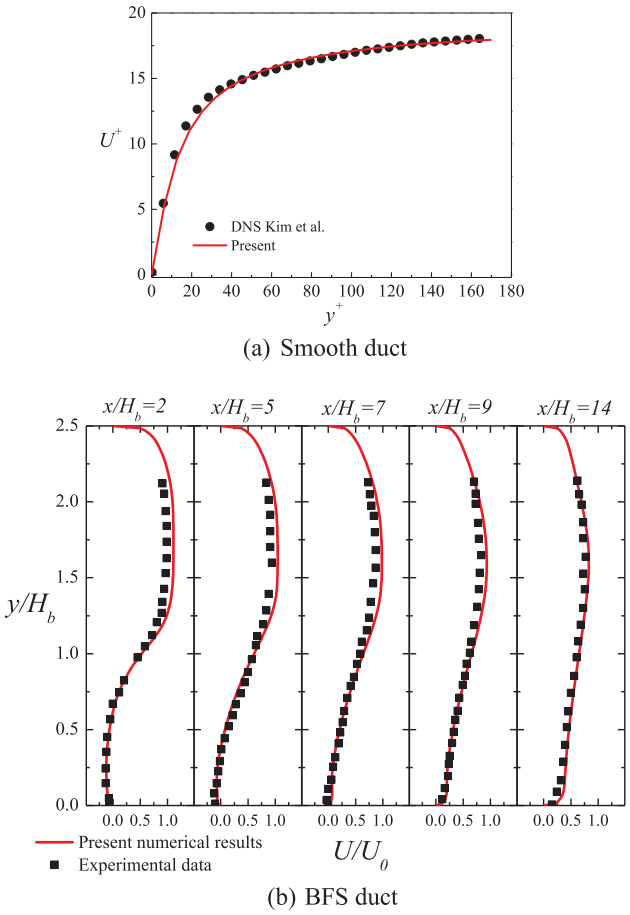

Fig. 4. Verification of mean air flow velocities for smooth and BFS duct flows.

ducts, as shown in Fig. 2(a–c). Tian et al. conducted detailed grid independent study for particle deposition in duct flow [23]. They found that the accurate results could be predicted if the first mesh spacing was 0.05 mm and the increasing factor of grid spacing was 1.2. Except for referring from the study of Tian et al. [23], a grid independence check was conducted for the case of smooth duct, as shown in the Fig. 3. The computational grids were 200 × 60, 300 × 70 and 400 × 80 in the

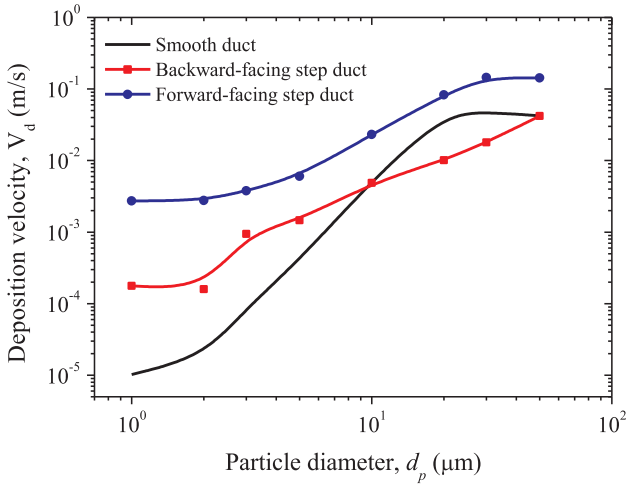

Fig. 6. Deposition velocity of particles in smooth, FFS and BFS dusts.

simulation. Particle deposition velocity profiles were obtained and compared for different grid resolution. It can be seen that the deposition velocities of particles are in good agreement between medium and fine grid cases. However, great difference can be observed between the coarse and medium grids. Therefore, the medium and fine grid resolution is accurate for predicting particle deposition in turbulent duct flow. The fine grid (400 × 80) was used in present study, thus the computational results are reliable. The computational cell numbers are 32000, 25786, 40,192 for smooth, FFS and BFS ducts respectively.

4. Results and discussions

4.1. Numerical Verification

Mean air velocities in smooth duct were obtained from the present simulation and compared with DNS results by Kim [35], as illustrated in Fig. 4(a). Moreover, several mean streamwise velocity profiles in BFS duct were validated with Fessler's experimental data [38], as displayed in Fig. 4(b). It can be found that the mean velocity profiles for smooth and BFS ducts both agree well with the literature results. Thus the present CFD models and computational grids can resolve both the smooth and BFS duct flow fields very well.

Furthermore, particle deposition velocity profile for smooth duct

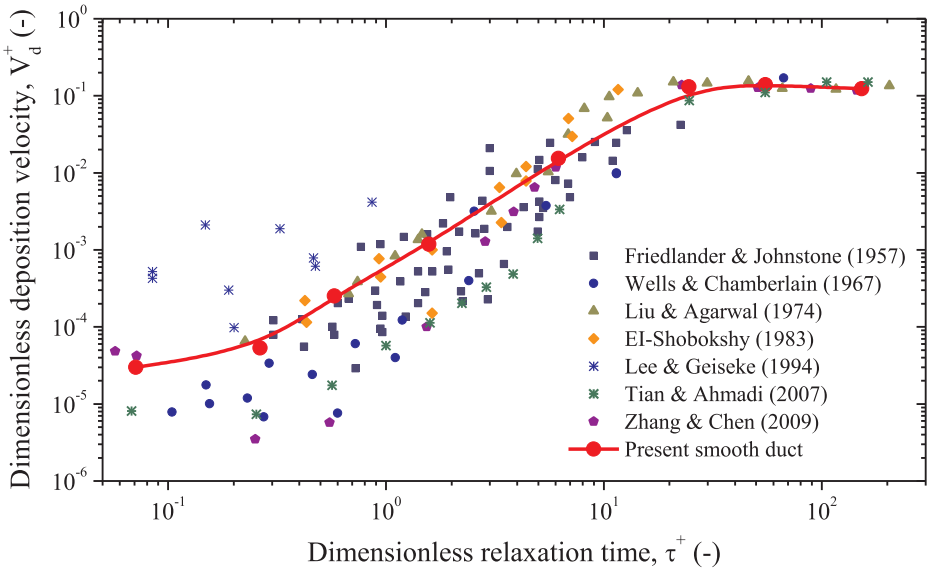

Fig. 5. Verification of particle deposition velocities in smooth duct.

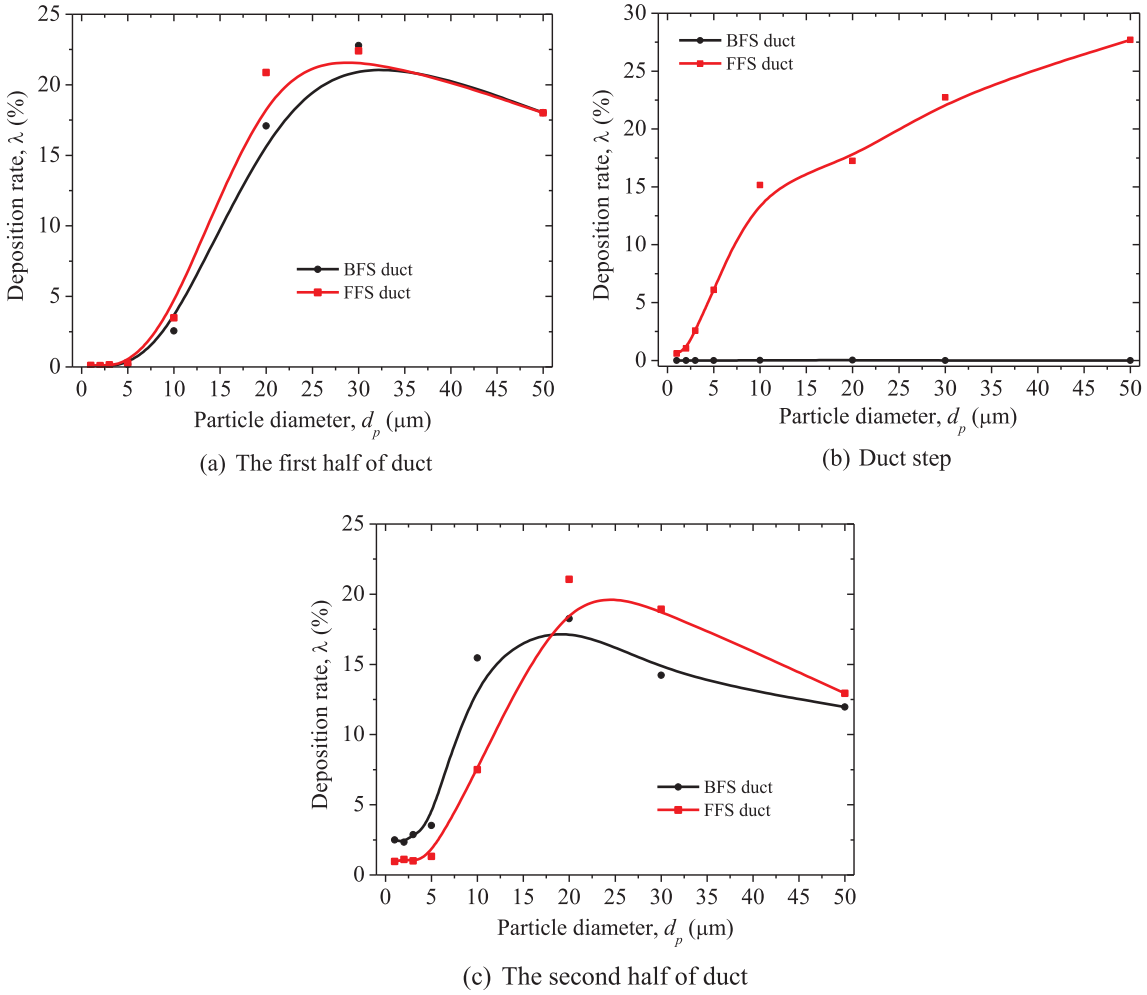

Fig. 7. Particle deposition rates in different sections of FFS and BFS ducts.

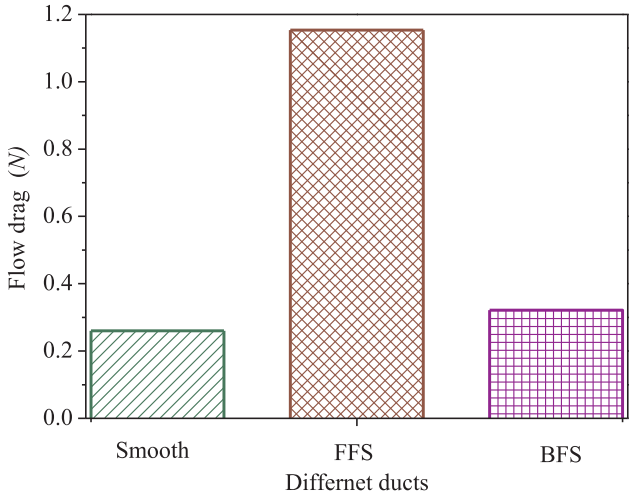

Fig. 8. Comparison of flow drags in smooth, FFS and BFS ducts.

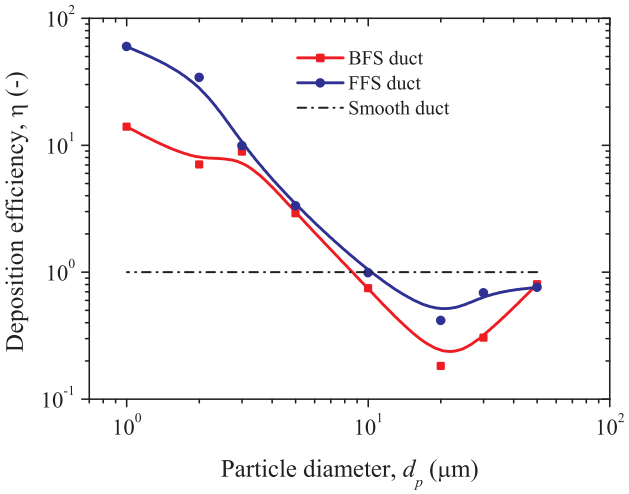

Fig. 9. Particle deposition efficiency in smooth, FFS and BFS dusts.

was verified by comparing previous experimental and numerical data [23,24,39–43], as shown in Fig. 5. The particle deposition velocity was calculated as follows [23,24],

$$V_d = \frac{J}{C_0} = \frac{N_d/t/A}{N_0/V} \tag{19}$$

where J is particle deposition number for unit time and area. C_0 is mean particle concentration. The particle deposition velocities in Fig. 5 were non-dimensionalized by using the friction velocity u^*. It can be seen that particle deposition velocity firstly rises and then keeps constant as particle relaxation time increases. Flow eddy diffusion and particle inertia are two main mechanisms of particle deposition in smooth duct. Moreover, the present deposition velocity profile is in good agreement with previous literature data. Thus present Eulerian-Lagrangian

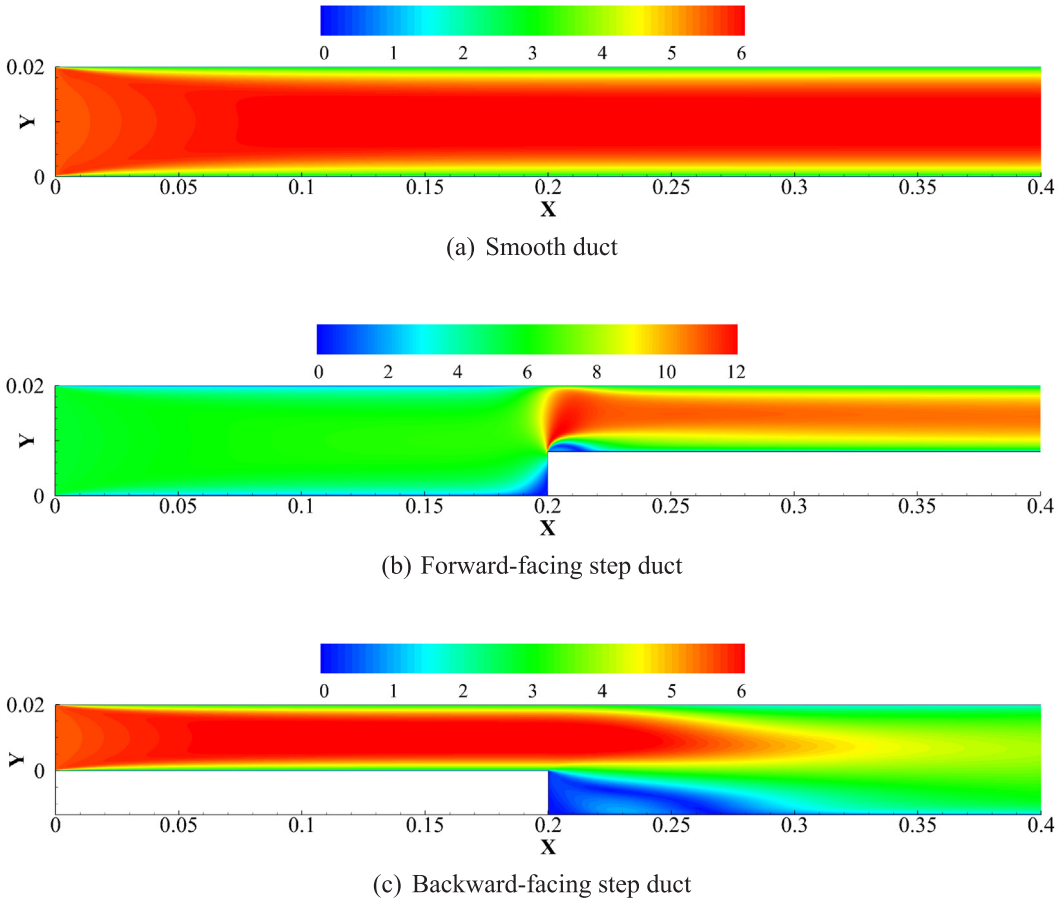

Fig. 10. Flow velocity fields for smooth, FFS and BFS ducts.

approach with velocity fluctuation correction is able to correctly model particle deposition behaviors. Therefore, the above numerical validations indicate that the numerical models in this study are correct and accurate.

4.2. Deposition velocity of particles

Deposition velocities of particles in smooth, FFS and BFS ducts were obtained and compared in Fig. 6. The curves of particle deposition velocities for FFS and BFS ducts are quite similar. The deposition velocity significantly rises when particle diameter increases. However, the deposition velocity curves for FFS and BFS ducts are significantly different from smooth duct case. Thus particle deposition behaviors and mechanisms are greatly modified by the FFS and BSF structures. For the FFS duct, particle deposition velocity profile for whole particle sizes are higher than the smooth duct case. However, increase degree of deposition velocity is obviously disparate for different size particles. Deposition velocity of FFS duct is much higher for small-size particles ($d_p < 10\,\mu$m), while the different of deposition velocities become small for large-size particles ($d_p > 10\,\mu$m), compared with smooth duct. A cross point of deposition velocity curves for smooth and BFS ducts can be observed in Fig. 6. The corresponding particle size for the cross point is 10 μm. When particle size is smaller than 10 μm, the deposition velocities for BFS duct are greater compared with smooth duct. However, the deposition velocities of BFS duct are lower than those of smooth duct for large particles ($d_p > 10\,\mu$m). Therefore, particle deposition characteristics in FFS and BFS ducts are strongly modified by duct geometry. The detailed mechanism of particle deposition in FFS and BFS ducts was examined in the next section.

To further investigate particle deposition behaviors clearly, the deposition rates in different sections of the FFS and BFS ducts were obtained and shown in Fig. 7. Particle deposition rates for the first half of duct, the step and the second half of duct were displayed in Fig. 7(a–c) respectively. From Fig. 7(a), particle deposition rates in the first half of FFS duct are quite similar with the first half of BFS duct. This is because the flow velocity and duct geometry are the same for the first half of FFS and BFS ducts. The maximum deposition rates are 22.7% and 22.4% for the first half of FFS and BFS ducts respectively. The according particle sizes are both 30 μm for FFS and BFS duct cases. Moreover, it can be observed that particle deposition rates on FFS duct step are much higher than those on BFS duct step. For BFS duct step, particle deposition rates are nearly zero for different particle sizes. Because the BFS step is in the leeward position and particles are hard to reach the step surface. However, particle deposition rate on FFS duct step is significantly increased when particle diameter increases. The maximum particle rate on FFS duct step can reach 27.7% for 50 μm particles. This indicates that many particles are intercepted by windward step surface. Furthermore, when particle size is less than 10 μm, particle deposition rates for the second half of BFS duct are greater compared with the second half of FFS duct. However, the situation is opposite for large particles ($d_p > 10\,\mu$m). As a large-scale turbulent eddy is induced behind the BFS, the particle deposition rates for small particles are enhanced by the eddy capture and entrainment. Therefore, the second half of BFS duct has higher deposition rate for small particles, compared with the second half of FFS duct. Nevertheless, the width of the second half of FFS duct is smaller than that of the second half of BFS duct. Therefore, large particles are much easier to reach the walls for deposition in the second half of FFS duct.

4.3. Particle deposition efficiency

Particle deposition efficiency in duct flow needs to consider both

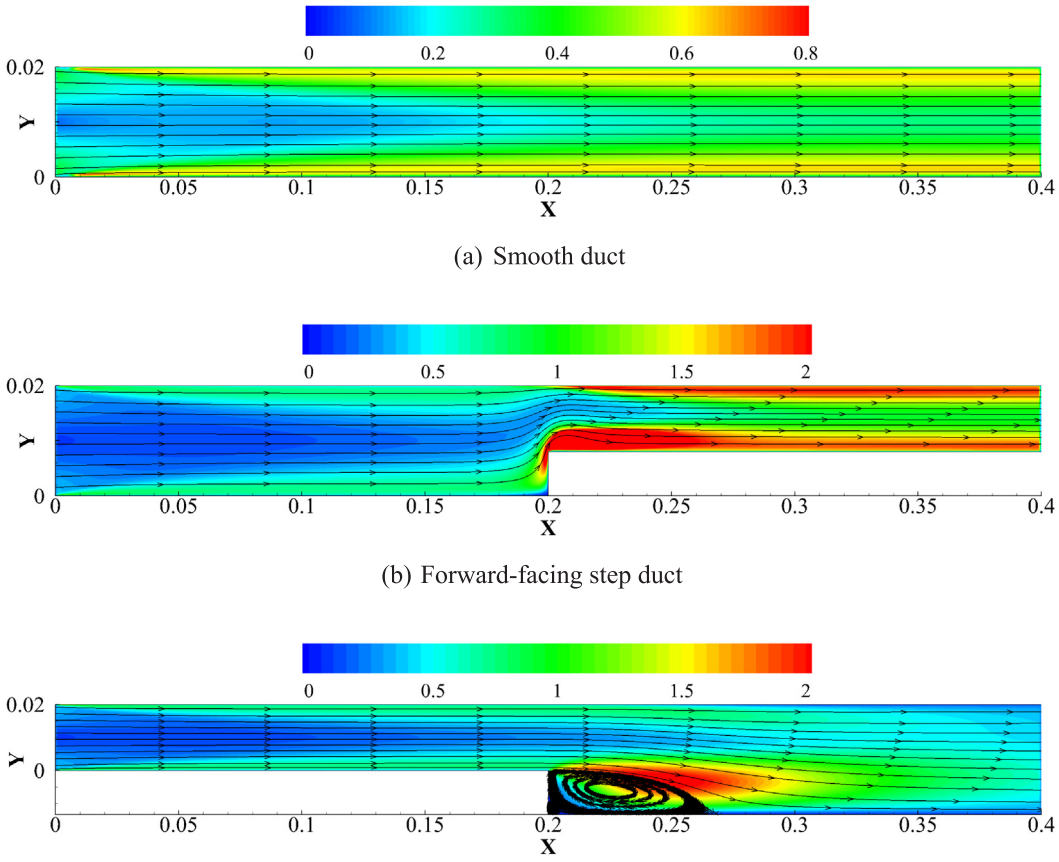

Fig. 11. Flow streamlines and TKE fields of air flow in smooth, FFS and BFS ducts.

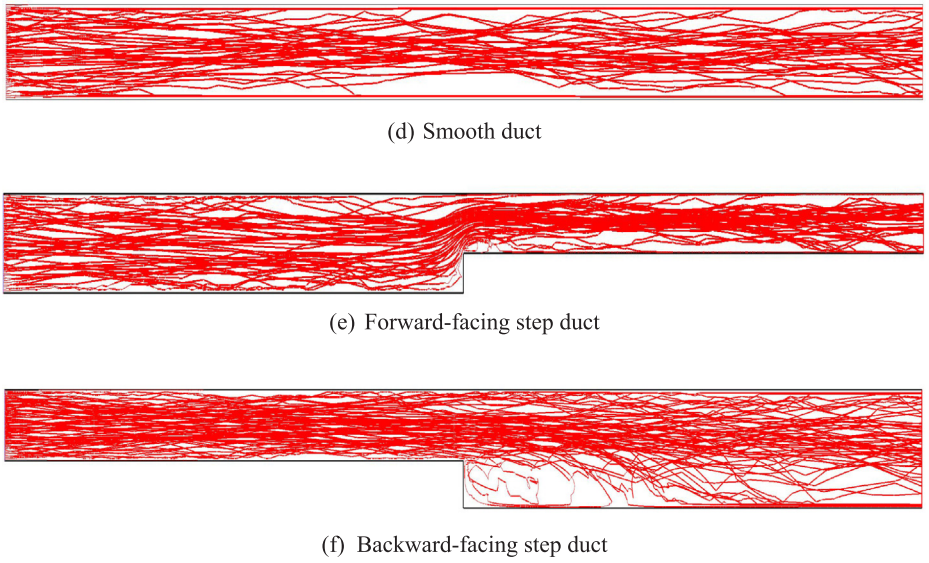

Fig. 12. Particle trajectories in smooth, FFS and BFS ducts for diameter of 1 μm.

deposition velocity and flow drag. The flow drags of FFS and BFS duct cases would be quite different from smooth duct. Fig. 8 displays the flow drags of smooth, FFS and BFS ducts. It can be observed that the flow drags are 0.26, 1.15 and 0.32 *N* for smooth, FFS and BFS ducts respectively. Flow drag of FFS or BFS duct is both larger than smooth duct. However, flow drag of FFS duct is much higher than that of BFS duct due to the form drag of windward step.

To compare particle deposition ability of smooth and BFS/FFS ducts, a particle deposition efficiency ratio was defined by considering the flow drag as follows [32–34],

$$\eta = \frac{v_{d\ rough}}{v_{dsmooth}} \cdot \frac{f_{smooth}}{f_{rough}} \tag{20}$$

where the f_{rough}/f_{smooth} is increase of flow drag. The deposition efficiency

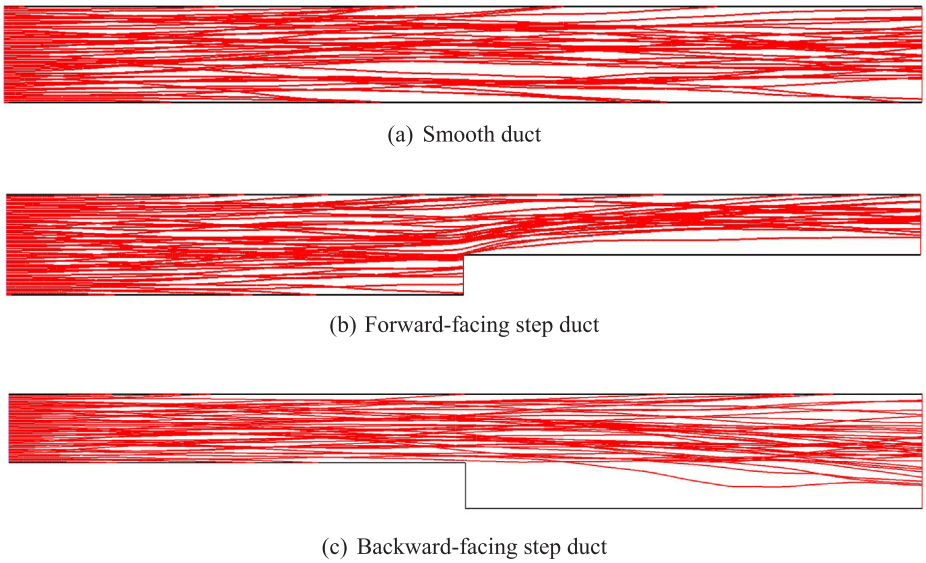

(a) Smooth duct

(b) Forward-facing step duct

(c) Backward-facing step duct

Fig. 13. Particle trajectories in smooth, FFS and BFS ducts for diameter of 50 μm.

ratios of smooth, FFS and BFS ducts were shown in Fig. 9. It can be found that deposition efficiency ratios of FFS and BFS ducts are higher than 1 for small particle sizes ($d_p < 10\,\mu$m) while lower than 1 for large particle sizes ($d_p > 10\,\mu$m). It indicates that FFS and BFS ducts can enhance particle deposition efficiency for small particles ($d_p < 10\,\mu$m). When particle size is 1 μm, the deposition efficiency reach the maximum for both FFS and BFS ducts. The according peak deposition efficiency ratio reaches 60 and 14 for FFS and BFS respectively. This implies that the FFS duct is more efficient to enhance particle deposition for small particles, especially for PM2.5 (fine particles less than 2.5 μm).

4.4. Deposition mechanisms of particles

To investigate deposition mechanisms of particles in FFS and BFS ducts, the air flow field structures and TKE distributions with streamlines in different ducts were obtained and displayed in Figs. 10 and 11 respectively. From the Fig. 10(a), it can be found that turbulent boundary layer in smooth duct is well resolved and flow field is fully developed. The air velocity distribution keeps constant and stable in the streamwise direction. However, the flow velocity fields for FFS and BFS ducts are quite complicated, as shown in Fig. 10(b) and (c). For FFS duct, the air velocity is suddenly increased to more than 10 m/s after the FFS because of the reduction of the duct cross-section width, as shown in Fig. 10(b). However, the air velocity decreases behind the BFS due to the expansion of the duct cross-section width, as shown in Fig. 10(c). Particle deposition in BFS duct would decrease when air velocity decreases. Conversely, the interception of step surface and increase of flow speed in FFS duct would enhance particle deposition. Therefore, the FFS duct has higher deposition velocity than BFS duct.

Moreover, Fig. 11 shows the streamlines and TKE distributions in smooth, FFS and BFS ducts. The color in the figure represents TKE value. From Fig. 11(a), the streamlines are parallel with the flow direction. The TKE values are large near the wall and the peak value is 0.7 J/kg. However, the streamlines are dramatically changed for FFS duct, as shown in Fig. 11(b). The TKE values are more intense in FFS and the maximum TKE value reaches 2 J/kg, which can greatly enhance particle deposition. For BFS duct, it can be observed that a large-scale separated turbulent vortex is produced behind BFS. A large number of particles can be trapped by the turbulent vortex and transported for deposition, especially for small particles. Therefore, BFS duct can enhance deposition rate for small particles.

Particle trajectories in smooth, FFS and BFS duct flow were obtained and shown in Figs. 12 and 13. The particle sizes are 1 and 50 μm in the Figs. 12 and 13 respectively. When particle diameter is 1 μm, it can be found that particle trajectories can fill in the whole geometry for all types of ducts, as shown in Fig. 12(a–c). Moreover, the particle trajectories cross with each other because the particle inertia is quite small and turbulent eddies have great influences on particle motions. However, particle trajectories are much different for large particles of 50 μm. From Fig. 13(a), the particle trajectories are hardly modified by flow vortex because of high inertia. Moreover, there is a region behind the FFS or BFS that no any particle trajectories can reach there, as shown in Fig. 13(b) and (c). This phenomenon is the “particle free zone” [44]. Small particles are difficult to form “particle free zone”, as they can well follow air flow streamlines. However, this effect can be caused by the high inertia of particles and specific duct geometry.

5. Conclusions

Particle deposition in FFS and BFS ducts were studied numerically by Reynolds stress model and discrete particle model. To improve prediction accuracy of particle deposition, turbulent velocity fluctuation was corrected near the wall. Moreover, fully developed velocities and TKE distributions were applied at the inlet of the ducts. After numerical validation, particle deposition velocities and mechanisms as well as deposition efficiency ratios considering flow drag in BFS and FFS ducts were investigated carefully. The conclusions are as follows,

1. The deposition velocity of FFS duct is higher than smooth duct by one or two orders of magnitude, especially for small particles ($d_p < 10\,\mu$m). For BFS duct, particle deposition velocity is greater for small particles ($d_p < 10\,\mu$m) but lower for large particles ($d_p > 10\,\mu$m), compared with smooth duct cases.

2. For BFS duct, it can be observed that a large-scale separated turbulent vortex is produced behind BFS. Many particles are trapped by the turbulent vortex and transported to the wall for deposition, especially for small particles. The increase of flow speed and interception of step surface for FFS duct can increase particle deposition. Therefore, the FFS duct has higher deposition velocity than BFS duct.

3. FFS and BFS ducts could increase particle deposition efficiency for small particle sizes ($d_p < 10\,\mu$m), compared with smooth duct. When particle size is 1 μm, the deposition efficiency ratio reaches the maximum for both FFS and BFS ducts. The according peak deposition efficiency ratios are 60 and 14 for FFS and BFS ducts respectively.

Acknowledgement

The authors appreciate the financial supports provided by the National Natural Science Foundation of China (Grant Nos. 50876053).

References

[1] Yang X, Ingham D, Ma L, Williams A, Pourkashanian M. Predicting ash deposition behaviour for co-combustion of palm kernel with coal based on CFD modelling of particle impaction and sticking. Fuel 2016;165:41–9.
[2] Pérez MG, Vakkilainen E, Hyppänen T. The contribution of differently-sized ash particles to the fouling trends of a pilot-scale coal-fired combustor with an ash deposition CFD model. Fuel 2017;189:120–30.
[3] Yang X, Ingham D, Ma L, Zhou H, Pourkashanian M. Understanding the ash deposition formation in Zhundong lignite combustion through dynamic CFD modelling analysis. Fuel 2017;194:533–43.
[4] Jin HH, Fan JR, Zeng MJ, Cen KF. Large eddy simulation of inhaled particle deposition within the human upper respiratory tract. J Aerosol Sci 2007;38:257–68.
[5] Salimifard P, Rim D, Gomes C, Kremer P, Freihaut JD. Resuspension of biological particles from indoor surfaces: Effects of humidity and air swirl. Sci Total Environ 2017;583:241–7.
[6] Gao NP, Niu JL. Modeling particle dispersion and deposition in indoor environments. Atmos Environ 2007;41:3862–76.
[7] Jin HH, He C, Lu L, Fan JR. Numerical investigation of the wall effect on airborne particle dispersion in a test chamber. Aerosol Air Qual Res 2013;13:786–94.
[8] Wood NB. A simple method for the calculation of turbulent deposition to smooth and rough surfaces. J Aerosol Sci 1981;12:275–90.
[9] Fan F, Ahmadi G. A sublayer model for turbulent deposition of particles in vertical ducts with smooth and rough surfaces. J Aerosol Sci 1993;24:45–64.
[10] Othmane MB, Havet M, Gehin E, Solliec C. Mechanisms of particle deposition in ventilation ducts for a food factory. Aerosol Sci Technol 2010;44:775–84.
[11] Sippola MR, Nazaroff WW. Experiment measuring particle deposition from fully developed turbulent flow in ventilation ducts. Aerosol Sci Technol 2004;38:914–25.
[12] Dehbi A. A CFD model for particle dispersion in turbulent boundary layer flows. Nucl Eng Des 2008;238:707–15.
[13] Zhao B, Chen JJ. Numerical analysis of particle deposition in ventilation duct. Build Environ 2006;41:710–8.
[14] Gao NP, Niu JL, He QB, Zhu T, Wu JZ. Using RANS turbulence models and Lagrangian approach to predict particle deposition in turbulent channel flows. Build Environ 2012;48:206–14.
[15] Gao R, Li A. Modeling deposition of particles in vertical square ventilation duct flows. Build Environ 2011;46(1):245–52.
[16] Zhang J, Li A. Study on particle deposition in vertical square ventilation duct flows by different models. Energy Convers Manage 2008;49(5):1008–18.
[17] Lai ACK, Nazaroff WW. Modelling indoor particle deposition from turbulent flow onto smooth surfaces. J Aerosol Sci 2000;31:463–76.
[18] Zhao B, Wu J. Modeling particle deposition from fully developed turbulent flow in ventilation duct. Atmos Environ 2006;40:457–546.
[19] Zhao B, Wu J. Modeling particle deposition onto rough walls in ventilation duct. Atmos Environ 2006;40:6918–27.
[20] Uijttewaal WSJ, Oliemans RVA. Particle dispersion and deposition in direct numerical and large eddy simulations of vertical pipe flows. Phys Fluids 1996;8:2590–604.
[21] Zhang H, Ahmadi G. Aerosol particle transport and deposition in vertical and horizontal turbulent duct flows. J Fluid Mech 2000;406:55–80.
[22] Yao J, Fairweather M. Particle deposition in turbulent duct flows. Chem Eng Sci 2012;84:781–800.
[23] Tian L, Ahmadi G. Particle deposition in turbulent duct flows-comparisons of different model predictions. J Aerosol Sci 2007;38:377–97.
[24] Zhang Z, Chen Q. Prediction of particle deposition onto indoor surfaces by CFD with a modified Lagrangian method. Atmos Environ 2009;43:319–28.
[25] Sippola MR, Nazaroff WW. Particle deposition in ventilation ducts: connectors, bends and developing turbulent flow. Aerosol Sci Technol 2005;39:139–50.
[26] Sippola MR, Nazaroff WW. Modeling particle loss in ventilation ducts. Atmos Environ 2003;37:5597–609.
[27] Lustfeld M, Qu T, Lippmann W, Hurtado A, Göhler D. Experimental study of graphite particle deposition upstream of a forward-facing step. Nucl Eng Des 2014;271:552–9.
[28] Benedetto A, Russo P, Sanchirico R, Sarli V. CFD simulations of turbulent fluid flow and dust dispersion in the 20 liter explosion vessel. AIChE J 2013;59(7):2485–96.
[29] Sarli V, Russo P, Sanchirico R, Benedetto A. CFD simulations of dust dispersion in the 20 L vessel: effect of nominal dust concentration. J Loss Prev Process Ind 2014;27:8–12.
[30] Sarli V, Russo P, Sanchirico R, Di Benedetto A. CFD simulations of the effect of dust diameter on the dispersion in the 20 l bomb. Chem Eng Trans 2013;31:727–32.
[31] Lu H, Lu L, Jiang Y. Numerical simulation of particle deposition in duct air flows with uniform, expanding or contracting cross-section. Energy Build 2016;128:867–75.
[32] Lu H, Lu L. Numerical investigation on particle deposition enhancement in duct air flow by ribbed wall. Build Environ 2015;85:61–72.
[33] Lu H, Lu L. Effects of rib spacing and height on particle deposition in ribbed duct air flows. Build Environ 2015;92:317–27.
[34] Lu H, Lu L. A numerical study of particle deposition in ribbed duct flow with different rib shapes. Build Environ 2015;94:43–53.
[35] Kim J, Moin P, Moser R. Turbulence statistics in fully developed channel flow at low Reynolds number. J Fluid Mech 1987;177:133–66.
[36] Lecrivain G, Drapeau-Martin S, Barth T, Hampel U. Numerical simulation of multilayer deposition in an obstructed channel flow. Adv Powder Technol 2014;25:310–20.
[37] Partankar SV: Numerical heat transfer and fluid flow. Hemisphere, Washington, DC, 1980.
[38] Fessler JR, Eaton JK. Turbulence modification by particles in a backward-facing step flow. J Fluid Mech 1999;394:97–117.
[39] Friedlander SK, Johnstone HF. Deposition of suspended particles from turbulent gas streams. Ind Eng Chem 1957;49:1151–6.
[40] Wells AC, Chamberlain AC. Transport of small particles to vertical surfaces. Br J Appl Phys 1967;18:1793–9.
[41] Liu BYH, Agarwal JK. Experimental observation of aerosol deposition in turbulent flow. J Aerosol Sci 1974;5:145–55.
[42] El-Shobokshy MS. Experimental measurements of aerosol deposition to smooth and rough surfaces. Atmos Environ 1983;17:639–44.
[43] Lee KW, Gieseke JA. Deposition of particles in turbulent pipe flows. J Aerosol Sci 1994;25:699–709.
[44] Sun K, Lu L, Jiang H. A numerical study of bend-induced particle deposition in and behind duct bends. Build Environ 2012;52:77–87.